CONF-961017--14

THE MECHANICAL PROPERTIES OF FeAl

I. Baker[#] and E.P. George[†]
[#]Thayer School of Engineering, Dartmouth College, Hanover, NH 03755
[†]Metals and Ceramics Division, Oak Ridge National Laboratory, Oak Ridge, TN 03781

Abstract

Only in the last few years has considerable progress been made in obtaining reproducible mechanical properties data for FeAl. Two sets of observations are the foundation of this progress. The first is that the large vacancy concentrations that exist in FeAl at high temperature are easily retained at low temperature and that these strongly affect the low-temperature mechanical properties. The second is that room temperature ductility is adversely affected by the presence of water vapor. The purpose of this paper is not to present a comprehensive overview of the mechanical properties of FeAl but rather to highlight our understanding of key phenomena and to show how an understanding of the factors which control the yield strength and fracture behavior has followed from the discovery of the above two effects.

Introduction

FeAl is a B2 or ordered body-centered-cubic compound that exists over a large compositional range, from 36.5 to 49.5 at. % Al at room temperature, and up to a maximum temperature of 1583 K (at 46 at. % Al) (1). Iron-rich deviations from the stoichiometric composition are accommodated by Fe anti-site atoms. In addition, triple defects - two vacancies on the Fe sublattice site with an antisite (Fe) atom on the other (Al) sublattice - are present, especially in near-stoichiometric compositions (2). Irrespective of Fe:Al ratio, slip in FeAl occurs by the movement of anti-phase boundary (APB) coupled a/2<111> dislocations at low temperature but by the glide of perfect <100> dislocations at high temperature, see Figure 1. The temperature of this transition appears to decrease with increasing aluminum concentration (3-6). Slip occurs on {112} or {110} at low temperature but at room temperature and above slip is on {110} (3,7-21).

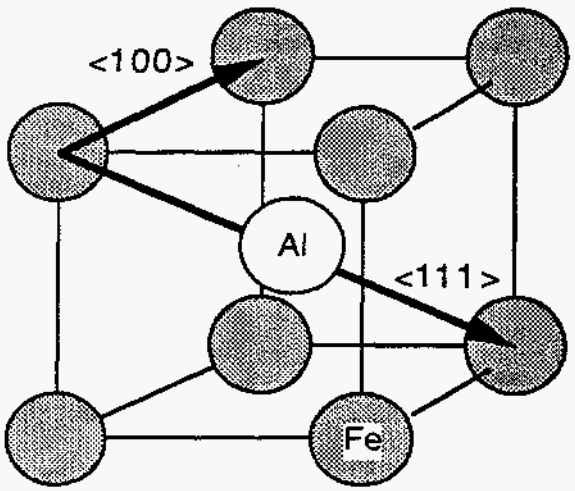

Figure 1. The B2 structure adopted by FeAl, showing the slip vectors at low temperature, <111>, and high temperature, <100>.

The mechanical properties of FeAl were first reported as long ago as 1956 (22), but it is only in the last few years that progress has been made in obtaining reproducible mechanical data. Two sets of observations are the foundation of this recent progress. The first is that the large vacancy concentrations that exist in FeAl at high temperature are easily retained at low temperature (23) and that these strongly affect the low-temperature mechanical properties (23-25), see Figure 2. The second is that room temperature ductility is reduced by water vapor (26).

DISCLAIMER

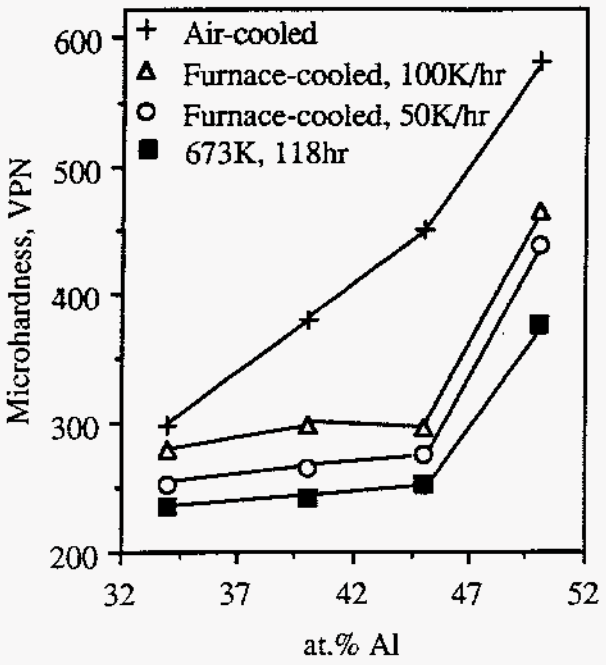

Figure 2. Graph of microhardness versus Al concentration in FeAl alloys after 1000 K anneals and various subsequent heat treatments. After reference 23.

The purpose of this paper is to highlight our understanding of the key phenomena for FeAl and to show how these flowed from the discovery of the above two effects.

Vacancy Effects

The substantial retention of vacancies, even after slow cooling following elevated temperature annealing, and their effect on mechanical properties was not noted until 1989 (24). It is now known that a low-temperature, long-term anneal (23) (typically, five days at 673 K for binary FeAl) will remove most of these vacancies and allow the intrinsic mechanical properties of FeAl to be determined. Without such an anneal, now routinely used by researchers on FeAl, it becomes impossible to compare different data since the vacancy effects dominate the strength and ductility, see Table I. In fact, the much-quoted early data by Westbrook (22) on the hardness of FeAl is, perhaps, misleading since it does not take into account vacancy effects. Once the importance of residual vacancies was noted, great strides were made in understanding the mechanical properties of FeAl, particularly regarding the compositional dependence of the room-temperature yield strength and the temperature dependence of the yield stress for a given composition.

Heat-Treatment	Elongation (%)	Strength (MPa)
As-extruded	0	790
Air cool	0	622
Furnace cool	0.7	554
Air cool + 673K anneal	1.1	312
Furnace cool+ 673K anneal	1.6	261

Table 1. Elongation and strength of large-grained Fe-45Al annealed at 1273K and after various subsequent heat-treatments (27). The stregths indicated are yield strengths except when no plastic elongation occurred, when they are fracture strengths.

Room-Temperature Strength

Chang et al. (28) calculated the room-temperature equilibrium vacancy concentrations in FeAl, arising from triple defects, and showed that the dependence of the vacancy concentration on the Fe:Al ratio was very similar to the hardness dependence on this ratio, implying that the vacancies controlled the room-temperature yield strength.

Later, Xiao and Baker (29) measured the vacancy concentrations at room temperature as a function of Fe:Al ratio and demonstrated the close similarity of this dependence with the dependence of the yield strength on Fe:Al ratio, see Figure 3. The room temperature yield strength behavior now seems to be reasonably well understood except for the details of the vacancy strengthening mechanism in FeAl.

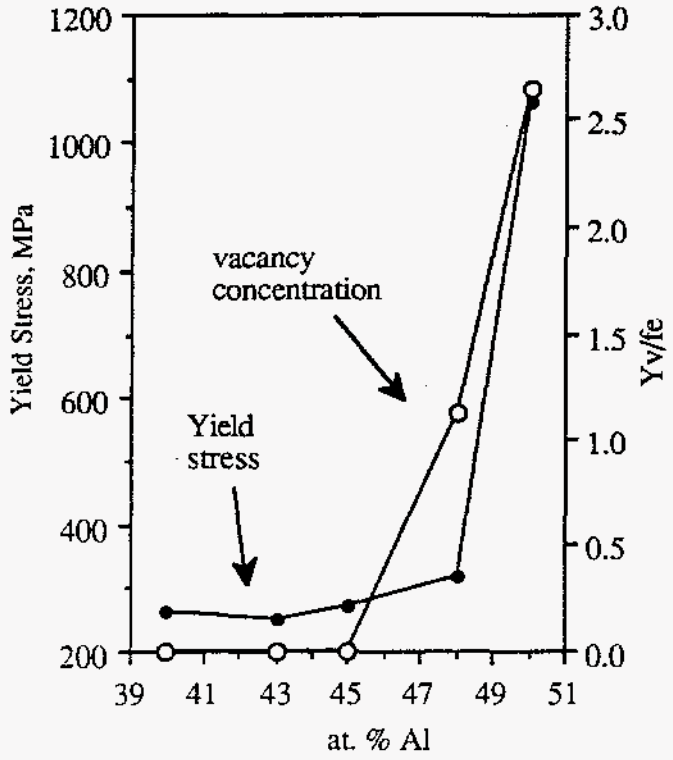

Figure 3. Graph of yield stress and percentage vacancy concentration on iron sites, $Y_{v/fe}$, versus aluminum concentration for large-grained low-temperature-annealed FeAl. After reference 29.

Chang et al. (28) also demonstrated that the hardness showed a square-root dependence on the concentration of quenched-in vacancies irrespective of Fe:Al ratio, see Figure 4. This behavior might be anticipated if there is no change in slip behavior with increasing vacancy concentration (see below). If vacancies pin the dislocations causing them to bow out, then the strength increase due to vacancies is proportional to the reciprocal of their spacing on the slip plane, λ. Since λ is roughly proportional to $C_v^{-1/2}$, where C_v is the vacancy concentration, the experimentally-observed parabolic relationship between hardness and C_v is obtained.

Whilst Figure 4 is quite useful from a practical standpoint, the yield strength and strain-hardening rate (both of which determine the hardness) are not described by such a simple functional relationship (30), see Figure 5. This is because vacancy clustering may occur and high vacancy concentrations lead to a change in dislocation behavior, e.g. cross-slip is promoted (30) which results in a substantially-reduced hardening rate with further increases in vacancy concentration.

A final point concerns the effect of grain boundaries on the room temperature strength. It has been shown that the Hall-Petch slope, a measure of grain boundary strengthening, has a maximum at the stoichiometric composition (even though this is the only composition to show cross-slip (27)) and decreases on the iron-rich side of this composition. This trend is similar to the variation of the lattice resistance with aluminum concentration (31). Whilst the latter behavior can be related to the vacancy concentration, it is unlikely that vacancies control the grain boundary strength. Thus, the origin of the dependence of the grain boundary strengthening behavior on aluminum concentration is unclear. The unusual dependence of the Lüders strain at room temperature, ε_L, on the grain size, d, *viz.*, $\varepsilon_L \alpha d^{-1.4}$ for both Fe-34Al and Fe-40Al, and $\varepsilon_L \alpha d^{-1.9}$ for Fe-45Al, where for a given grain size the Lüders strain increases in the order Fe-45Al > Fe-40Al > Fe-34Al (Lüders yielding does not occur at the stoichiometric composition) (31,32) is also unclear.

The Yield Strength Anomaly

By removing the residual vacancies in large-grained FeAl (which strengthen FeAl at low temperature but weaken it at high temperature) and using large-grained material (to minimize the effects of grain boundaries which strengthen at low temperature but weaken at high temperature), Xiao and Baker (33) showed that polycrystalline iron-rich FeAl exhibits a yield strength peak with increasing temperature, i.e., a so-called yield strength anomaly. A small peak was also present in the earlier data of Baker and Gaydosh (34) on Fe-37Al-2Ni and later noted in directionally-solidified FeAl by Chang (35). Subsequently, this yield strength peak, which occurs at around 0.45 T_m, where T_m is the homologous melting temperature, was reported in several other papers in which the effect of strain rate, single crystal orientation and Fe:Al ratio were examined (36-45), see, for example, Figure 6.

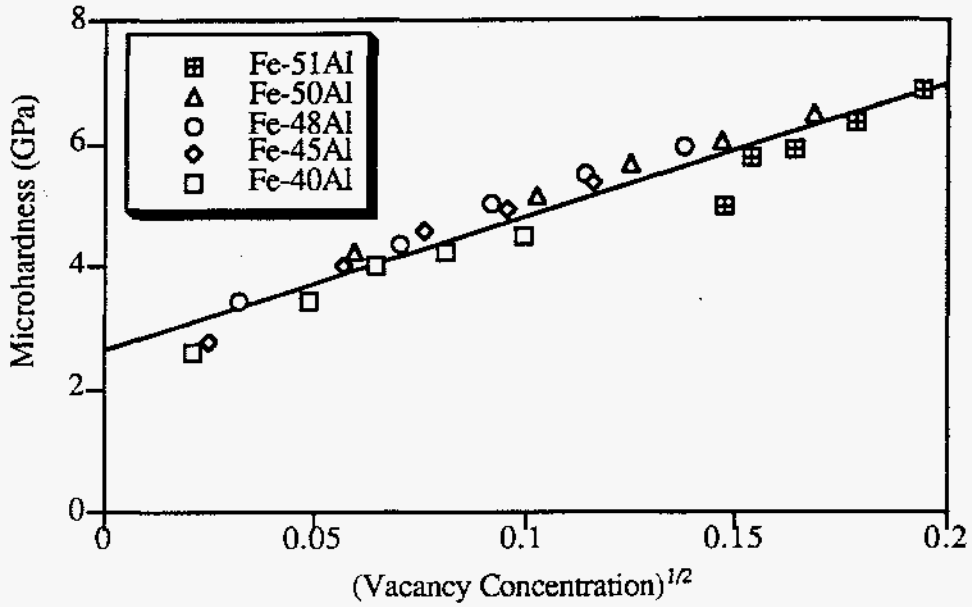

Figure 4. Graph of microhardness versus (vacancy concentration)$^{1/2}$ for FeAl polycrystals quenched from various temperatures. After reference 28.

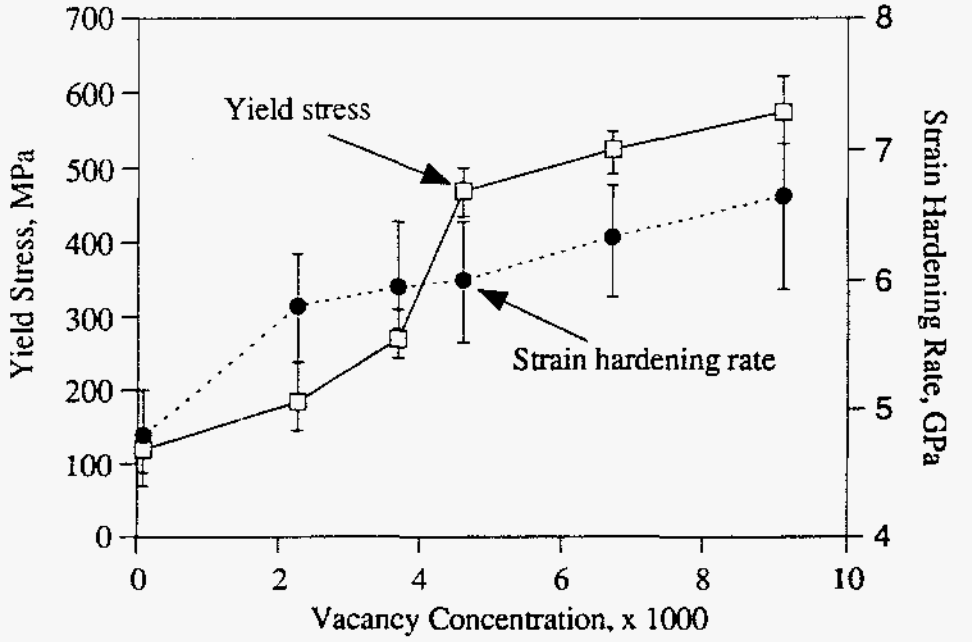

Figure 5. Graph of yield stress and strain hardening rate as a function of vacancy concentration for single-slip oriented single crystals of Fe-40Al. After reference 30.

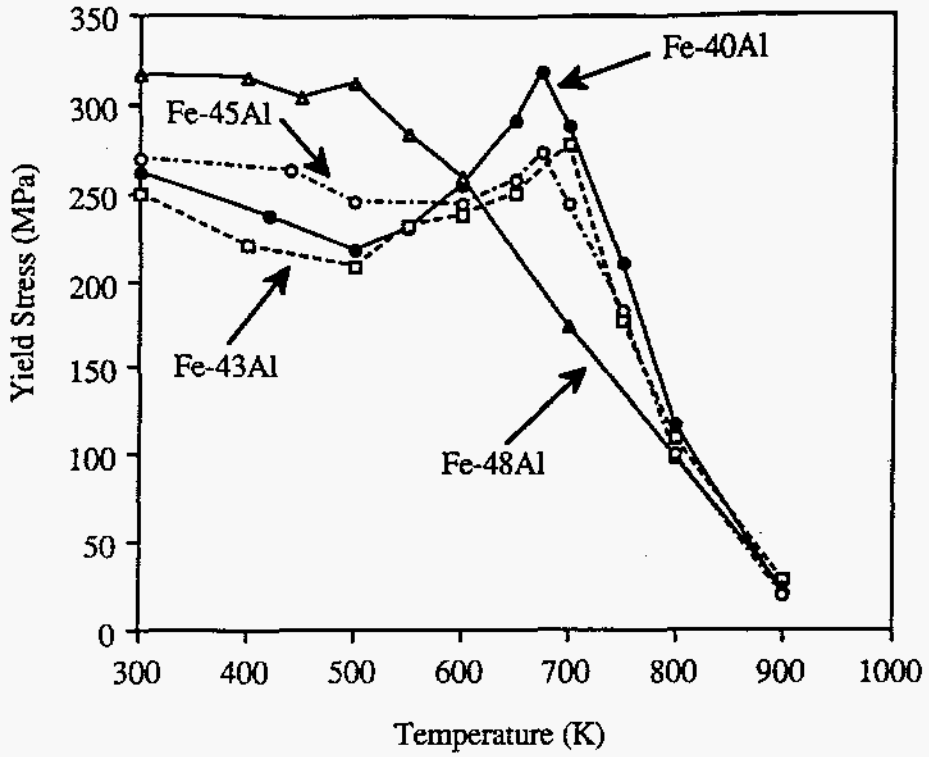

Figure 6. Graph of yield strength vs. temperature for large-grained, low-temperature annealed, off-stoichiometric FeAl strained under tension at 1 x 10^{-4} s^{-1}. After Baker et al. (41).

Three models have been proposed to explain this so-called anomalous temperature dependence of the yield strength exhibited by FeAl: the local climb-lock model (46); the dislocation decomposition model (36); and the vacancy hardening model (47). (The APB-dragging and cross-slip pinning models, which have been used to explain the yield stress peak as a function of temperature observed in a number of weakly-ordered B2 compounds, seem quite inappropriate for FeAl (43)). Prior to the introduction of any of these models, it was noted (33) that the anomalous yield stress peak occurred around the temperature of the <111> to <100> slip transition. However, this transition alone can not explain the yield peak for two reasons. First, the (homologous) temperature at which the yield peak is observed is approximately independent of Fe:Al ratio (41,43) but the slip transition temperature increases with increases in this ratio (48), see Figure 6. Second, there has to be a mechanism whereby <111> slip becomes more difficult with increasing temperature for a yield peak to occur (a slip transition would presumably simply produce a change in the slope of the yield stress-temperature curve). Thus, each of the three models noted above has a means whereby movement of the APB-coupled a/2<111> dislocations is impeded by a mechanism whose propensity increases with increasing temperature. Each model will be briefly outlined.

The Local Climb Lock Model

In the local climb lock model by Morris (46), local climb and realignment of APB-coupled a/2<111> edge partials is thought to occur in order to minimize their self-energy (the driving force for the process), with the result that some dislocation segments do not have their APB lying on the slip plane. The activation barrier associated with the process arises because the APB length and, hence, energy clearly increases from the initial to the final dislocation configurations. Dragging the climbed segments leads to an increased critical resolved shear stress (CRSS) for <111> slip. Greater climb and, hence, a larger density of climb-locked dislocation segments will occur with increasing temperature. Hence, the CRSS for <111> slip rises with increasing temperature until the point at which <100> slip becomes easier (the CRSS for <100> slip decreases continuously with increasing temperature (3)) and takes over. This gives rise to the yield peak.

A problem with the model is that the yield stress peak is expected to occur at lower temperatures with increases in aluminum concentration, due to changes in APB energy (46). Experimental observations, see Figure 7, do not appear to bear this out: at a strain rate of 1 x 10^{-4} s^{-1}, the yield peak occurs at about the same temperature for all

iron-rich alloys but decreases in magnitude whereas near-stoichiometric Fe-48Al does not show a yield strength peak. The model also implies a strain rate dependence in the anomalous region (since climb dissociation is not instantaneous) contrary to experimental observations (45).

The Dislocation Decomposition Model

In this model (36), segments of a<111> dislocations dissociate into a<100> and a<011> segments. The latter two dislocations are not mobile in FeAl at temperatures below the yield peak temperature and pin the <111> dislocation. Since recombination of the a/2<111> partials must occur before the a<111> dislocation can dissociate and because this requires thermal activation, the decomposition will occur more readily at higher temperatures. This produces a greater number of pinning points and, hence, more difficult <111> slip with increasing temperature, until <100> slip intervenes. Thus far, this dislocation decomposition has not been observed in FeAl even through a search for it was the focus of a recent paper (49). The dislocation decomposition model suffers from the problem that as the strain rate is decreased, more dissociated segments might be expected and, hence, the yield peak should increase in magnitude but occur at a lower temperature, as <100> slip intervenes. This is inconsistent with experiments, see Figure 7.

The Vacancy-Hardening Model

George and Baker (47) divided the relationship between the yield stress and temperature for FeAl into four regions, see Figure 7. Their vacancy-hardening model for the yield stress anomaly (47) is based on the idea (43) that immediately below the yield strength peak (Region III on Figure 7) vacancies are essentially immobile and impede dislocation motion (see earlier), and that above the peak (in Region IV) the vacancies are able to migrate and, hence, aid dislocation climb. Using the approximation (28) that the increase in strength from the vacancies is proportional to (vacancy concentration)$^{1/2}$ and knowing that the vacancy concentration increases exponentially with increasing temperature, it was shown that the strength increase with increasing temperature up to the yield strength peak was proportional to $\exp[-E_f/2kT]$, where E_f is the activation enthalpy of formation of vacancies, k is Boltzmann's constant and T is the absolute temperature. Above the yield strength peak, the ability of vacancies to migrate produces dislocation creep. Thus, at constant strain rate, the strength above the peak is approximately proportional to $\exp[E_D/mkT]$, where m is a material constant, E_D is the activation enthalpy for diffusion (= E_f + E_m), where E_m is the activation enthalpy of vacancy migration. A prominent yield strength peak is thus expected for a material where E_f is low relative to E_m, i.e. vacancies are easily formed but migrate with difficulty until higher temperatures. This is, indeed, the case for FeAl where E_f and E_m have been measured to be 95 kJ/mol and 164 kJ/mol, respectively (50). Mathematically fitting experimental data for Fe-40Al to their model, George and Baker (47) obtained a value of E_f of 92 kJ/mol, which is close to the experimentally-determined value determined using other techniques (50), and a reasonable value of m for dislocation creep of 3.8.

According to this model (47), the yield strength below the peak is approximately independent of strain rate whereas above the peak, in the dislocation creep regime, the yield strength has a strain rate, $\dot{\gamma}$, dependence proportional to $\dot{\gamma}^{1/m}$. It follows that the yield strength peak should itself be strain rate dependent, the peak moving to higher stresses and higher temperatures with increasing strain rate and to lower stresses and lower temperatures with decreasing strain rate, see Figure 7. This prediction is borne out in practice (43,51) and at very low strain rates the yield peak can even not be present at all. The model is also consistent with the observation that the time held at the peak yield stress temperature prior to testing affects the magnitude of yield stress at that temperature (45). This effect arises because vacancy formation is not instantaneous but requires time, with increasing times (which result in greater vacancy concentrations) leading to larger yield stresses (45).

A further interesting implication of this model is that it does not require the slip vector transition from <111> to <100> with increasing temperature. Rather the slip transition is a by-product of the vacancy hardening of <111> slip. Hence, the model may have more general applicability than simply to an alloy where this slip transition occurs.

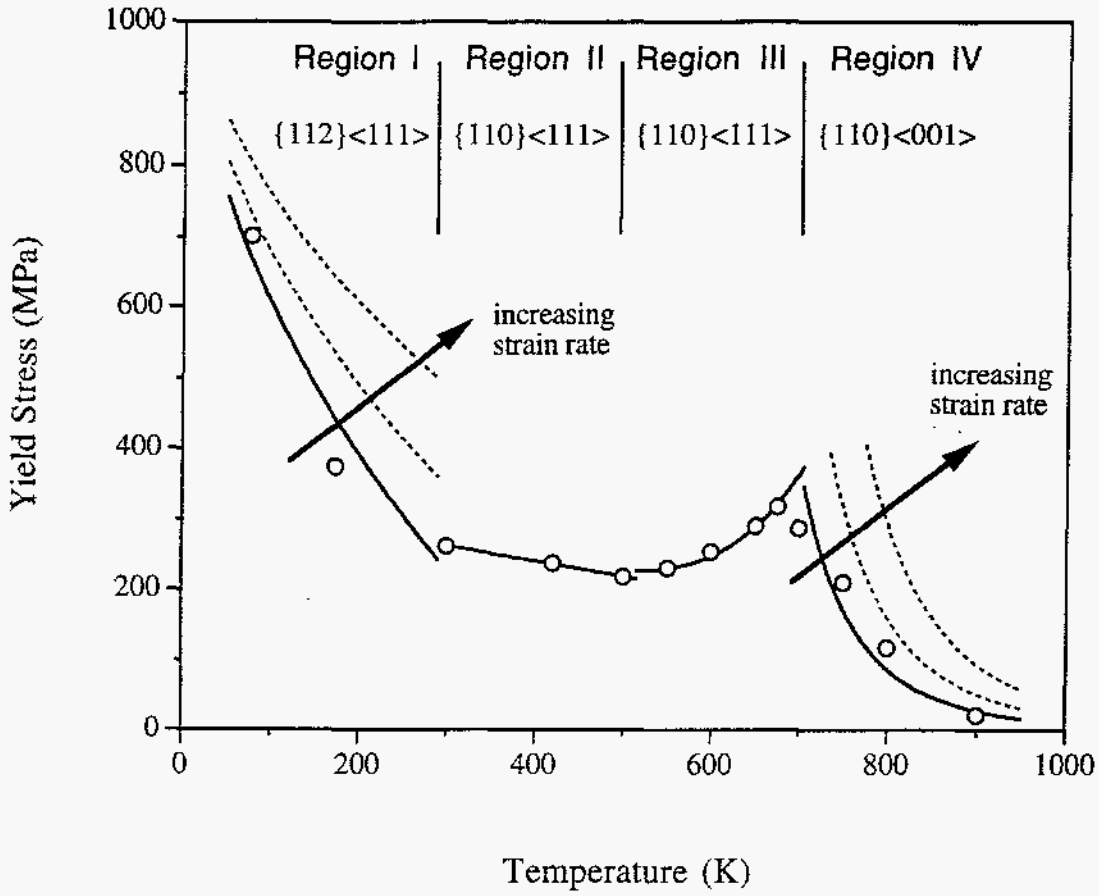

Figure 7. Schematic showing the yield stress versus temperature for FeAl separated into four regions. The slip systems are shown (52,53) as are the effects of strain rate, which are only important in Regions I and IV.

Finally, Yoshimi et al. (42,44) have recently noted a tension/compression asymmetry in the yield strength of Fe-39Al single crystals. In tension, crystals oriented near <100> show the yield stress peak at a lower temperature than other orientations whilst in compression crystals oriented near <111> exhibit the yield stress peak at the lowest temperature. The origin of this behavior is at present unclear but is presumably related to the effect of the hydrostatic stress component on the dislocation core.

The Environmental Effect

The effect of environment on the mechanical properties of FeAl was first noted by Liu, Lee and McKamey (26) for Fe-37Al. This alloy exhibited 2% elongation and transgranular cleavage in air; 5.5% elongation and mixed mode failure in vacuum; and 18% elongation and intergranular fracture in dry oxygen. (The yield strength was independent of the testing environment.) Liu et al. (26,54-56) proposed that the low ductility observed during tensile testing was due to local embrittlement at advancing crack tips from hydrogen arising from the reaction: $3H_2O + 2Al \rightarrow Al_2O_3 + 6H$. Indeed, subsequently moisture has been shown to reduce both the fracture toughness and to increase crack growth rates in FeAl (57-63).

The effect, which has now been shown to be common to many aluminides and silicides (64,65), is so pervasive that the effects of microstructural or alloying changes on mechanical properties are largely overwhelmed by it (66-68), see Figure 8. Hence, to study the effect of metallurgical variables on the intrinsic mechanical properties one has to test under conditions where the water vapor embrittlement does not occur, i.e. either in a benign atmosphere (e.g. argon, oxygen or vacuum), or at strain rates too fast for the environment to be important. Under such conditions, it has been demonstrated that reductions in grain size and the addition of boron can improve ductility, in all but the stoichiometric composition (64,66-68), see Figure 8.

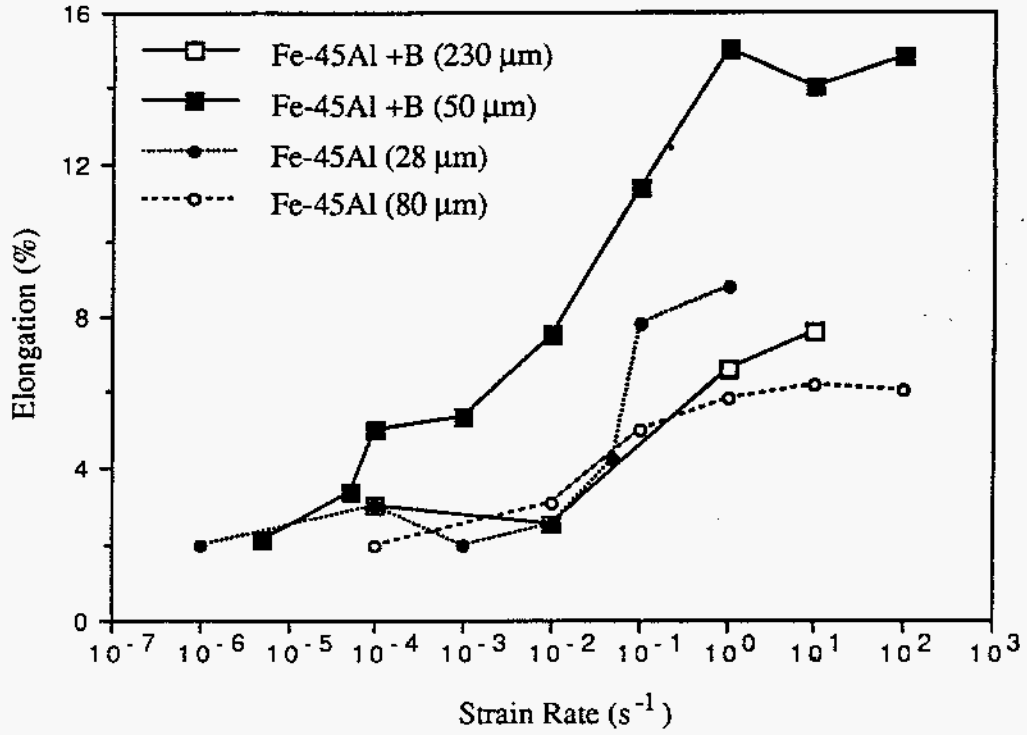

Figure 8. Elongation versus strain rate for both boron-doped and undoped, low-temperature-annealed Fe-45Al of different grain sizes tensile tested in air (68). At high strain rates (≥ 1 s^{-1}) the effects of grain size and of boron on the elongation of Fe-45Al are evident but at slow strain rates ($<1 \times 10^{-4}$ s^{-1}) their influence is overcome by the environment.

On the other hand, the ductility of FeAl for a given heat-treatment or environmental condition decreases with decreasing Fe:Al ratio (69) (until at 50 at. % Al no tensile elongation is observable in polycrystals), the effect of environmental moisture/hydrogen (and of residual vacancies) being to simply reduce the overall magnitude of the ductility, see Figure 9. The ductility of FeAl increases with increasing temperature irrespective of Fe:Al ratio with the fracture mode also changing with increasing temperature from transgranular cleavage to ductile rupture for iron-rich alloys but from intergranular fracture to transgranular cleavage to ductile rupture for near-stoichiometric alloys (41,43).

Thus far, unlike Ni_3Al (70), no solution has been developed to mitigate the environmental embrittlement problem in FeAl. (Boron additions prevent intergranular fracture in iron-rich FeAl, but fracture still occurs at low strains in the presence of water vapor (56)). And unlike Ni_3Al, where environmental embrittlement causes intergranular fracture (71), in FeAl the presence of water vapor can produce either premature intergranular or transgranular fracture depending on the Fe:Al ratio and possibly grain size (25,26,54-60,66-68). Indeed, even single crystals are susceptible to environmental embrittlement (32,61,62,72-74) although there is some disagreement over whether the environment affects the fracture plane.

Environmental Embrittlement Mechanisms

The phenomenology of the environmental embrittlement of FeAl has been covered in a number of reviews (75-78). Here, we point out some of the salient features of recent research which provide clues to the embrittling mechanisms involved:

i) Kasul and Heldt (79), by measuring crack growth velocity in air for B2-ordered Fe-35Al, determined the critical velocity for environmental embrittlement to be ~7 x 10^{-5} $m.s^{-1}$. Crack velocities greater than this were not affected by the environment.

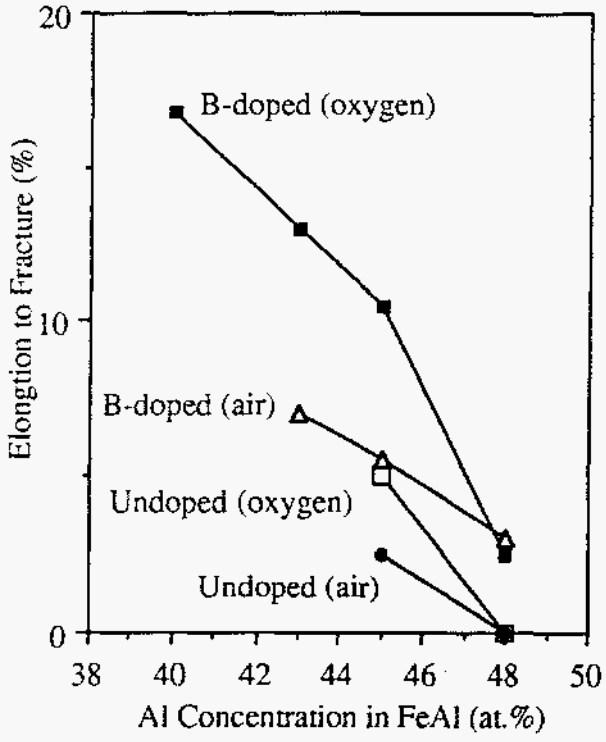

Figure 9. Effect of aluminum concentration and test environment on the room temperature tensile ductility of B-doped and B-free FeAl. After reference 69.

ii) Fractography of tensile-tested iron-rich FeAl specimens, which show intergranular fracture in vacuum and transgranular cleavage in air (26,55,56,66,67), show the same fracture mode all the way across the gauge. This suggests either that hydrogen uniformly embrittles the specimen or that the strain rates are such that the hydrogen generation reaction can keep pace with the growing crack, i.e. the hydrogen doesn't have to diffuse very far.

iii) Kasul and Heldt (79), by examining the effect of hydrogen charging and subsequent degassing at elevated temperature on the room-temperature fracture of Fe-35Al, estimated that the diffusion coefficient of hydrogen in FeAl at room temperature is ~4 x 10^{-16} m^2s^{-1}. A problem with this estimation is that it assumes the same diffusion mechanism at room temperature as at elevated temperatures. (They also found increasing transgranular cleavage for increasing hydrogen content.) However, this low diffusivity of hydrogen suggests either that the hydrogen embrittlement (which affects the whole specimen, see ii)) is not due to hydrogen transport by diffusion (it has been suggested that moving dislocations might assist diffusion and have an affect on the dislocation structure (79,80)) or that the embrittlement is a near surface phenomenon.

iv) Li and Liu (81) modeled the temperature dependence of the environmental embrittlement of Fe-36.5Al and concluded that the rate-controlling process was the reaction between the water vapor and the aluminum. (It has been shown that the dissociation of hydrogen molecules at the surface of FeAl is facilitated by iron (82)). In other words, diffusion of hydrogen into the material did not control the process.

v) Gleason et al. (83), using x-ray photoelectron spectroscopy and ultraviolet photoelectron spectroscopy, confirmed that hydrogen was produced from water vapor at the surface of FeAl, and that alloying elements, such as boron, affect the dissociation rate. They also noted that the hydrogen absorption and dissociation is mostly influenced by the iron.

vi) Through first principles calculations of the cohesive energy, Yoo and Fu (84) have shown that fracture of FeAl cannot be by elastic fracture (the measured fracture toughness values are too high (57-62,74)). A fact corroborated by the

observed tensile elongation prior to failure even in water-vapor embrittled FeAl (26,55,56,66,67) and the inability to obtain electron channeling patterns from fracture surfaces of all compositions (85) except stoichiometric FeAl. Stoichiometric FeAl typically fractures in tension at around one half to one third of the yield stress measured in compression (85).

vii) Robertson and Birnbaum (86) used TEM *in-situ* straining in an environmental cell to show that wet gases lead to changes in the mobility of dislocations in the related compound Fe_3Al. (The effect was reversible.) They suggested that hydrogen locally enhanced plasticity, reducing the local yield stress and causing highly localized deformation. This is consistent with the highly localized deformation at the fracture surface observed by Gaydosh and Nathal (25) for a FeAl single crystal tested in air.

viii) Munroe and Baker (87) suggested, based on their TEM observations, that <100> dislocations produced by interaction of gliding <111> dislocations might nucleate cleavage cracks on {100}, the observed fracture plane (74). Thus, Li and Liu (81) suggested that hydrogen could lower the energy of <100> dislocations and, hence, aid their formation. Note that whilst this crack nucleation mechanism produces an initial transgranular crack, subsequent crack propagation could be either transgranular or intergranular. Interestingly, whilst polycrystalline Fe-43Al (56), Fe-45Al (85) and Fe-48Al (41) fracture intergranularly at room temperature some transgranular cleavage areas do occur on fracture surfaces (41).

From the above observations one can conclude that the rate-controlling process in the environmental embrittlement of FeAl is the formation of atomic hydrogen from water vapor, a process that may be affected by alloying. How crack nucleation occurs is unclear. It may be by the <100> dislocation formation mechanism suggested by Munroe and Baker (87), which may be enhanced by hydrogen (81). However, surface imperfections and specimen flaws can always provide crack nucleation sites. The rôle of hydrogen on the crack propagation process is unclear. Diffusion of hydrogen appears to be too slow to aid crack propagation (79). One possibility, therefore, is that the embrittlement occurs very near the surface and hydrogen does not have to diffuse very far. Another possibility, to which several observations point, is that hydrogen is transported into the material by gliding dislocations (79,80). Understanding this process would be very valuable for improving the environmental resistance of iron aluminides through alloying additions and/or thermomechanical processing. Decreasing the environmental susceptibility of these alloys will extend the range of their potential industrial applications.

Conclusions

In the last few years, two features of the mechanical behavior of FeAl have become well established, *viz.*, the environmental effect and that vacancies control the strength. Understanding these phenomena has enabled a greater understanding of the fracture behavior of FeAl and allowed such features as the yield strength anomaly to be observed.

Acknowledgments

This work was supported by the Division of Materials Sciences, U.S. Department of Energy, through contract DE-FG02-87ER45311 with Dartmouth College and contract De-AC05-96OR22464 with Lockheed Martin Energy Research Corporation.

References

1. T.B. Massalski, ed., "Binary alloy phase diagrams", 112; 1986, Metals Park, OH, ASM.
2. J.P. Neumann, Y.A. Chang and C.M. Lee, Acta Metall., 1976, A, **24**, 593.
3. Y. Umakoshi and M. Yamaguchi, Phil. Mag., **41** (1980) 573.
4. M.G. Mendiratta, H.K. Kim, and H.A. Lipsitt: *Metall. Trans. A*, 1984, **15A**, 395.
5. I. Baker and D.J. Gaydosh: *Mater. Sci. Eng.*, 1987, **96**, 147.
6. P. R. Munroe and I. Baker: *J. Mat. Sci.*, 1989, **24**, 4246.
7. Y. Umakoshi and M. Yamaguchi: *Phil. Mag. A*, 1981, **44**, 711.
8. M.A. Crimp and K. Vedula: *Phil. Mag. A*, 1991, **63**, 559.
9. T. Yamagata and H. Yoshida: *Mater. Sci. Eng.*, 1973, **12**, 95.
10. I.L.F. Ray, R.C. Crawford, and D.J.H. Cockayne: *Phil. Mag.*, 1970, **21**, 1027.
11. R.C. Crawford, *Phil. Mag.*, 1976, **33**, 529.
12. T. Yamagata: *Trans. JIM*, 1977, **18**, 715.
13. S. Takeuchi: *Phil. Mag. A*, 1980, **41**, 541.
14. P.R. Munroe and I. Baker: *Acta Metall. Mater.*, 1991, **39**, 1011.
15. C.T. Chou and P.B. Hirsch: *Phil. Mag. A*, 1981, **44**, 1415.
16. C.T. Chou and P.B. Hirsch: in Inst. Phys. Conf. Series, 1982, **61**, 459.
17. C.T. Chou and P.B. Hirsch: Proc. R. Soc., 1983, **A387**, 91.
18. P.M. Hazzledine and P.B. Hirsch: in Proc. MRS, Vol. 81, 75; 1987.
19. I. Baker and D.J. Gaydosh: in Proc. MRS, Vol. 81, 315; 1987.
20. R.C. Crawford and I.L.F. Ray: *Phil. Mag.*, 1977, **35**, 549.
21. J.T. Kandra, R. Mahapatra and E.W. Lee: *Mat. Sci. Eng.*, 1993, **A170**, 29.
22. J.H. Westbrook, J. Electrochem. Soc., **103** (1956) 54.
23. P. Nagpal and I. Baker, Metall. Trans., **21A** (1990) 2281.
24. B. Schmidt, P. Nagpal and I. Baker, Proc. MRS, **133** (1989) 755.
25. D.J. Gaydosh and M.V. Nathal, Scripta Metall. Mater., **24** (1990) 1281.
26. C.T. Liu, E.H. Lee and C.G. McKamey, Scripta Metall., **23** (1989) 875.
27. O. Klein and I. Baker: *Scripta Metall. Mater.*, 1994, **30**, 627.
28. Y.A. Chang, L.M. Pike, C.T. Liu, A.R. Bilbrey and D.S. Stone, Intermetallics, **1** (1993) 107.
29. H. Xiao and I. Baker, Acta Metall. Mater., **43** (1995) 391.
30. Y. Yang and I. Baker, submitted to Phil. Mag.
31. I. Baker, P. Nagpal, F. Liu, and P.R. Munroe: *Acta Metall. Mater.*, 1991, **39**, 1637.
32. D.J. Gaydosh, S.L. Draper, R.D. Noebe and M.V. Nathal, Mater. Sci. Eng., **A150** (1992) 7.
33. H. Xiao and I. Baker, Scripta Metall. Mater., **28** (1993) 1411.
34. I. Baker and D. J. Gaydosh, Mater. Sci. Eng., **96** (1987) 147.
35. K.-M. Chang, Metall. Trans. A, **21A** (1990) 3027.
36. K. Yoshimi and S. Hanada, in Structural Intermetallics, ed. - R. Darolia, J.J. Lewandowski, C.T. Liu, P.L. Martin, D.B. Miracle and M.V. Nathal,. TMS Warrendale, (1993) 475.
37. J.T. Guo, O. Jin, W.M. Yin and T.M. Wang, Scripta Metall. Mater., **29** (1993) 783.
38. K. Yoshimi, N. Masumoto, S. Hanada and S. Watanabe, Proc. 3rd Japan. Int. SAMPE Symp. (1993) 1404.
39. O. Klein and I. Baker, Scripta Metall. Mater., **30** (1994) 1413.
40. K. Yoshimi , S. Hanada and H. Tokuno., Mat. Trans. JIM, **35** (1994) 51.
41. I. Baker, H. Xiao, O. Klein, C. Nelson and J.D. Whittenberger, Acta Metall. Mater., **43** (1995) 1723.
42. K. Yoshimi, S. Hanada and M.H. Yoo, Acta Metall. Mater., **43** (1995) 4141.
43. R.L. Carlton, E.P. George and R.H. Zee, Intermetallics, **3** (1995) 433.
44. K. Yoshimi, S. Hanada and M.H. Yoo, Intermetallics, **4** (1996) 159.
45. E.P. George, R.L. Carlton, J. Cohron and R.H. Zee, submitted to Intermetallics.
46. D.G. Morris, Phil. Mag., **71** (1995) 1281.
47. E.P. George and I. Baker, submitted to Phil. Mag. (1996).
48. M.G. Mendiratta, H.K. Kim and H.A. Lipsitt, Metall. Trans. A, **15A** (1984), 395.
49. P.R. Munroe and I. Baker, Phil. Mag., **72** (1995) 1301.
50. R. Würschum, C. Grupp and H.-E. Schaefer, Phys. Rev. Lett., **75** (1995) 97.
51. X. Li and I. Baker, submitted to Scripta Metall. Mater.
52. I. Baker and P. Nagpal, in "Structural Intermetallics", Ed.- R. Darolia, J.J. Lewandowski, C.T. Liu, P.L. Martin, D.B. Miracle and M.V. Nathal, TMS, Warrendale, Pa., (1993) 463.
53. I. Baker, in "Processing, Properties and Applications of Iron Aluminides, Ed.- J.H.

Schneibel and M.A. Crimp, TMS, Warrendale, Pa., (1994) 101.
54. C.T. Liu and C.G. McKamey, in High temperature aluminides and intermetallics, Ed.- S.H. Whang, C.T. Liu, D.P. Pope and J.O. Steigler, TMS, Warrendale, Pa., (1990) 133.
55. C.T. Liu and E.P. George, Scripta Metall. Mater., **24** (1990) 1285.
56. C.T. Liu and E.P. George, Proc. MRS, **213** (1991) 527.
57. O. Klein, I. Baker and P. Nagpal, Proc. MRS, **213** (1993) 609.
58. J.H. Schneibel and M.G. Jenkins, Scripta Metall. Mater., **28** (1993) 389.
59. J.H. Schneibel, M.G. Jenkins and P. J. Maziasz, Proc. MRS, **288** (1993) 549.
60. J.H. Schneibel and E.D. Specht, Scripta Metall. Mater., **31** (1994) 1737.
61. P. Specht, M. Brede and P. Neumann, Proc. MRS, **364** (1995) 207.
62. P. Specht and P. Neumann, Intermetallic, **3** (1995) 365.
63. A. Castagna and N.S. Stoloff, Mater. Sci. Eng., **A192/193** (1995) 399.
64. E.P. George and C.T. Liu, Proc. MRS, **364** (1995) 1131.
65. C.T. Liu, in Ordered Intermetallics - Physical Metallurgy and Mechanical Behavior, ed. - C.T. Liu, R.W. Cahn and G. Sauthoff, Kluwer Publishers, Netherlands, (1992) 321.
66. P. Nagpal and I. Baker, Scripta Metall. Mater., **25** (1991) 2577.
67. O. Klein and I. Baker, Scripta Metall. Mater., **27** (1992) 1823.
68. I. Baker, O. Klein, C. Nelson and E. P. George, Scripta Metall. Mater., **30** (1994) 863.
69. E.P. George, M. Yamaguchi, K.S. Kumar and C.T. Liu, Ann. Rev. Mater., **24** (1994) 409.
70. C.T. Liu, Scripta Metall. Mater., **27** (1992) 25.
71. E.P. George, C.T. Liu and D.P. Pope, Scripta Metall. Mater., **28** (1993) 857.
72. R.J. Lynch, K.A. Gee and L.A. Heldt, Scripta Metall. Mater., **30** (1994) 945.
73. M. V. Nathal and C. T. Liu, Intermetallics, **3** (1995) 77.
74. K.-M. Chang, R. Darolia and H. A. Lipsitt, Acta Metall. Mater., **40** (1992) 2727.
75. N.S. Stoloff, in Hydrogen Effects on Material Behavior, TMS, Warrendale, PA, (1994).
76. N.S. Stoloff and C.T. Liu, Intermetallics , **2** (1995) 75.
77. E.P. George and C.T. Liu, Proc. MRS, **364** (1995) 1131.
78. X. Pierron and I. Baker, Proc. Symp. Physical Chemistry of High Temperature Composites, Intermetallics and Metal-Ceramic Systems", TMS, Warrendale, Pa., 1996.
79. D.B. Kasul and L.A. Heldt, Metall. Trans., **25A** (1994) 1285.
80. G.M. Camus, N. S. Stoloff and D. J. Duquette, Acta Metall., **37** (1989) 1497.
81. J.C.M. Li and C.T. Liu, Scripta Metall. Mater., **33** (1995) 661.
82. G.A. Somorjai, Chemistry in Two Dimensions: Surfaces, Cornell Univ. Press, Ithaca NY, 1981.
83. N.R. Gleason, C.A. Gerken and D.R. Strongin, Applied Surface Science, **72** (1993) 215.
84. M.H. Yoo and C.L. Fu, Mater. Sci. Eng., **A153** (1992)470.
85. P. Nagpal and I. Baker, Mater. Char., **27** (1991) 167.
86. I.M. Robertson and H.K. Birnbaum, unpublished results (1993).
87. P.R. Munroe and I. Baker, Acta Metall. Mater., **39** (1991) 1011.